PAPER

Influence of the mode of deformation on recrystallisation behaviour of titanium through experiments, mean field theory and phase field model

View the article online for updates and enhancements.

Influence of the mode of deformation on recrystallisation behaviour of titanium through experiments, mean field theory and phase field model

C N Athreya[1] , **A Mukilventhan[2], Satyam Suwas[3], Srikanth Vedantam[2] and V Subramanya Sarma[1]**

[1] Department of Metallurgical and Materials Engineering, Indian Institute of Technology Madras, Chennai 600036, India
[2] Department of Engineering Design, Indian Institute of Technology Madras, Chennai 600036, India
[3] Department of Materials Engineering, Indian Institute of Science, Bangalore 560012, India

E-mail: cnathreya@gmail.com

Abstract

The influence of the mode of deformation on recrystallisation behaviour of Ti was studied by experiments and modelling. Ti samples were deformed through torsion and rolling to the same equivalent strain of 0.5. The deformed samples were annealed at different temperatures for different time durations and the recrystallisation kinetics were compared. Recrystallisation is found to be faster in the rolled samples compared to the torsion deformed samples. This is attributed to the differences in stored energy and number of nuclei per unit area in the two modes of deformation. Considering decay in stored energy during recrystallisation, the grain boundary mobility was estimated through a mean field model. The activation energy for recrystallisation obtained from experiments matched with the activation energy for grain boundary migration obtained from mobility calculation. A multi-phase field model (with mobility estimated from the mean field model as a constitutive input) was used to simulate the kinetics, microstructure and texture evolution. The recrystallisation kinetics and grain size distributions obtained from experiments matched reasonably well with the phase field simulations. The recrystallisation texture predicted through phase field simulations compares well with experiments though few additional texture components are present in simulations. This is attributed to the anisotropy in grain boundary mobility, which is not accounted for in the present study.

(Some figures may appear in colour only in the online journal)

1. Introduction

Thermo-mechanical processing (TMP) is widely employed in metallic materials to achieve the desired shape and microstructure. During TMP, materials are subjected to cold/hot deformation and annealing cycles during which they undergo static/dynamic recovery/ recrystallisation. Also during TMP, materials undergo deformation under complex stress states obtained in rolling, forging, extrusion etc. During annealing, recovery, recrystallisation and grain growth are important mechanisms that control the microstructure [1]. Among these, recrystallisation has been widely investigated and exploited to control the microstructure. Recrystallisation is driven by the stored energy due to deformation and is strongly dependent on its spatial distribution [1, 2]. The magnitude of the stored energy and its spatial distribution depends on the mode of deformation. Of all the factors that influence the recrystallisation behaviour of material, the role of the mode of deformation on recrystallisation behaviour has not been studied in detail. The recrystallisation kinetics has been reported to be different in Mo, Al, Cu and Ni subjected to the same equivalent strain by different modes [3–8]. The differences have been attributed to the differences in stored energy, defect distribution, grain boundary character and deformation texture. In our recent work on Ni [9], samples deformed to the same von Mises equivalent strain through torsion was shown to have higher number density of probable nuclei, stored energy and fraction of high angle grain boundaries than samples deformed through rolling. For a given equivalent strain, Ni samples deformed through torsion recrystallised much faster than rolled samples [8].

α-Ti is a low symmetry HCP material with significant anisotropy and undergoes deformation through slip and twinning [10, 11]. The deformation texture [10] and stored energy [12] is strain path dependent in Ti. The propensity for slip and twinning is different for different initial orientations in tension and rolling [13, 14]. The strain hardening rate in Ti is deformation mode dependent [15]. The recrystallisation rate is reported to be different for Ti samples compressed to the same strain with different initial orientations and the difference is attributed to differences in slip and twin activity [16]. From these studies it is evident that the initial texture and mode of deformation is likely to have a significant effect on the deformation microstructure and recrystallisation behaviour of Ti. To the best of our knowledge, there are no studies on the influence of mode of plastic straining on the microstructure and the recrystallisation behaviour of Ti. The deformation microstructure in Ni and Ti subjected to torsion and rolling were reported in our recent study [17]. In the present study we investigate (through experiments and modelling) the influence of mode of deformation on static recrystallisation behaviour of Ti by deforming it through rolling and torsion to same equivalent strain.

Recrystallisation involves nucleation of strain free grains in the deformed matrix and their growth by the consumption of the deformed microstructure through the migration of high angle grain boundaries. To simulate and understand microstructural evolution during recrystallisation, various approaches such as cellular automata [18], Monte-Carlo [19] and phase field modelling [20–24] have been developed. Amongst these approaches, the phase field model appears to be amenable for the incorporation of the phenomenological aspects of mechanisms. Also, the model has the potential to handle complex geometry and morphology

with ease at lower computational expense. Moelans *et al* [20] have developed a phase field model to study the migration rate of a recrystallisation front. The model incorporates separate order parameters to describe the deformed grains and the recrystallised grain. In an alternative approach, we modified the coarse grain energy to account for stored energy along with the curvature based driving force [8]. To model the microstructure evolution during recrystallisation process, we consider the following three stages (i) recrystallisation nuclei are present in the deformed matrix (ii) growth of recrystallisation nuclei in a deformed microstrucutre and (iii) curvature driven grain growth after grain impingement. Site saturated initial nucleation process is considered. From the experimental data, the size, shape and spatial distribution of nuclei are taken as input.

In order to model the recrystallisation process, the grain boundary (GB) mobility is an important constitutive input and this data is not readily available in literature. The grain boundary mobility is estimated either through modelling or from specially designed experimental techniques. Molecular dynamic simulations are often used to estimate boundary mobility [25–27]. In these models, the misorientation dependent boundary mobility is determined based on bicrystal frame work. The grain growth is curvature driven and the driving force is maintained constant. To the best of our knowledge, these models do not consider decay in stored energy with time.

The most widely used experimental technique to estimate grain boundary mobility is through grain growth experiments in bi-crystal [25, 26, 28]. In these experiments, grain boundary mobility is estimated by tracking boundary migration under a constant driving force. The driving force for grain growth process is much lower compared to recrystallisation. In case of boundary migration during grain growth, boundaries interact with undeformed matrix. However, during recrystallisation, moving boundaries interact with dislocations in the deformed matrix and this will have effect on boundary mobility. The driving force for recrystallisation continuously decreases due to the consumption of deformed matrix by the grain growth of strain free grains and the concurrent occurrence of recovery in the deformed matrix. In this respect it is not very clear to what extent mobilities obtained from grain growth experiments and molecular dynamic simulations performed in bicrystal frame work is applicable to the recrystallisation process. Also, the GB mobility is misorientation dependent. As a result, it is difficult to estimate the GB mobility during recrystallisation. Vandermeer *et al* [29] have estimated the average grain boundary mobility during recrystallisation of copper combining the calorimetric and stereological measurements from EBSD data. In their work, the decay in stored energy was estimated through calorimetry of partially recrystallised samples. Grain boundary mobility can also be obtained by performing *in situ* annealing experiments in SEM chamber in order to track microstructure change with time [30]. However, it is important to note that the recrystallisation/grain growth kinetics is also affected by annealing atmosphere [31]. Hence, there is need to develop new experimental techniques and models to estimate GB mobility.

There are few studies employing mean field model to analyse the kinetics of grain growth and dynamic recrystallisation [32, 33]. These studies are based on the mean field model proposed by Hillert on grain growth [34]. Hurley and Humphreys [35] have used the mean field model to model recrystallisation by strain induced boundary migration. In their work, the grain boundary mobility obtained from *in situ* annealing experiments were used as input. In most of the studies, the grain boundary mobilities are not estimated and is taken from some experimental or modelling data. Favre *et al* [33], have estimated the boundary mobility during dynamic recrystallisation through mean field model. To the best of our knowledge, there are no reports on estimation of grain boundary mobility during static recrystallisation through mean field model.

Recently, we proposed a mean field model to estimate mean field GB mobility during recrystallisation considering the decay in stored energy [8]. The proposed model was similar to the classic model of Hillert which focussed on the statistical aspects of grain growth [34]. In the proposed model, mobility was estimated considering the decay in stored energy during recrystallisation with time using EBSD data. This provides a new method of calculating a mean-field mobility during recrystallisation. The obtained mean field GB mobility is used as constitutive input for the phase field model.

We organise the results in this paper as follows. We first present the recrystallisation experimental results of the deformed Ti samples. Next, we briefly summarise the multi-phase field model with the modified coarse grained free energy taking stored energy into account. The experimentally identified nuclei and stored energy data obtained from electron back-scatter diffraction (EBSD) are used as inputs into the multi-phase field model. For completeness, we briefly present the mean field model which is used for estimating the GB mobility. Finally, a detailed comparison of the simulations of the recrystallisation kinetics, grain size distribution and texture with the experimental results are presented and discussed.

2. Experimental details

CP Ti (grade 2) samples were machined out of an annealed extruded rod of 15 mm diameter for the rolling and torsion experiments. The samples were subjected to free end torsion up to von Mises equivalent strain (ε_{VM}) of 0.57 at which the sample failed. In torsion tested samples, the strain varies along radius and the region corresponding to strain of ε_{VM} of 0.5 was analysed. Ti samples were also deformed through rolling to 35% reduction (i.e., ε_{VM} of 0.5). The deformed specimens were isothermally annealed at 848, 873 and 898 K for different time durations in a tubular furnace. The samples were quenched immediately after heat treatment to preserve the high temperature microstructure. The microstructural characterisation of the deformed samples was carried out using EBSD. For characterisation using EBSD, samples were prepared through metallographic polishing with final stage of polishing being done with a mixture of 70% colloidal silica (0.05 μm) and 30% hydrogen peroxide. EBSD studies were carried out on a FEI make Inspect F FEGSEM equipped with high-speed HIKARI camera using TSL OIM™ data acquisition and post-processing software (ver 7.2). EBSD scans were performed (total area of $500 \times 500\ \mu m^2$ for rolled and $300 \times 400\ \mu m^2$ for torsion tested sample) with step size of 300 nm at 20 kV and 16 mm working distance. To identify potential nuclei in the deformed microstructure [9], few EBSD scans with step size of 50 nm were also performed. EBSD analysis was carried out on the central region of the RD-ND plane of rolled samples and in torsion-tested samples, on the Z–R sections corresponding to an average ε_{VM} of 0.5. The relevant sections for analysis in rolled and torsion tested samples are RD-TD section and Z–θ section respectively. The orientation of the rolled samples were rotated 90° about RD axis to obtain orientations corresponding to the RD-TD sections. Similarly, in the case of torsion deformed sample, orientations were rotated 90° about θ and Z axis, respectively. Based on the grain orientation spread (GOS) criterion of GOS < 2° [9], recrystallised regions were partitioned from EBSD maps. Recrystallisation fractions obtained from EBSD maps were used for analysis of recrystallisation kinetics and estimation of activation energy. For microtexture analysis, (0002) pole figures were calculated from the EBSD data based on harmonic series expansion method with series rank of 22 and Gaussian half-width of 5°. To calculate texture, orthotropic and triclinic sample symmetries were imposed on rolled and torsion samples, respectively.

3. Phase field model

We employ a phase field model that is capable of modelling recrystallisation by taking stored energy driving force into account in addition to the curvature based driving force. Similar phase field models have been proposed in the literature [22, 36]. These models employ Voronoi tessellation method for populating random grain structures. In the present work, the stored energy and nuclei distribution (number, size and shape) obtained from EBSD is explicitly mapped into the model. Similar work performed by Kamachali *et al* [37] assumes constant mobility. Our phase field model uses mobility obtained from experimental data and mean field model to account for the stored energy decay with annealing time. With this the advantages of our phase field model compared to the approaches mentioned above can be realised using experimentally realistic data.

We consider the case of microstructure evolution during recrystallisation from a highly deformed matrix through the growth of pre-existing nuclei that are already present in the deformed matrix. Our multiphase field model is based on that of Fan and Chen [23]. To represent individual nuclei, the model uses a list of order parameter fields $\{\eta_i\} = (\eta_1, \eta_2, ..., \eta_N)$. In particular, an order parameter field $\eta_i(r.t) = 1$ and $\eta_j(r, t) = 0 \ \forall \ j \neq i$ represent the *i*th nucleus. In the classical model proposed by Fan and Chen, unstable phase is represented by the state $\eta_j(r, t) = 0 \ \forall \ j \neq i$. In contrast, in our present model the state $\eta_j(r, t) = 0 \ \forall \ j$ is used to represent the deformed region.

The energy of the material is taken to be of the standard form

$$F = \int_V \sum_{i=1}^{N} \left\{ h(\{\eta_i\}) + \frac{\kappa}{2}\sum_i |\nabla \eta_i|^2 \right\} dV, \tag{1}$$

where κ is the gradient energy coefficient and $h(\{\eta_i\})$ is the coarse grained free energy which is taken to be of the form $h(\{\eta_i\}) = f(\{\eta_i\}) + g(\{\eta_i\})$. The key modification of our multiphase model is in the form of f which is taken to be a multiwell potential of unequal heights

$$f(\{\eta_i\}) = \mu \left[\alpha \left(\frac{\eta_i^2}{2} - \frac{\eta_i^3}{3} \right) + \frac{\eta_i^4}{4} - \frac{\eta_i^3}{3} \right], \tag{2}$$

where α is related to the stored energy of the deformed matrix. For two α values, $\Delta f = \mu(2\alpha - 1)/12$ gives the the difference in energy between the two wells. The second component of the coarse grained energy g is the standard post-impingement energy in multi-phase field models [23],

$$g(\{\eta_i\}) = \sum_{j>i}^{N} \frac{\lambda}{2}\eta_i^2 \eta_j^2. \tag{3}$$

The evolution of the order parameters are through the time dependent Ginzburg–Landau equations

$$\frac{\partial \eta_i}{\partial t} = -L\frac{\delta F}{\delta \eta_i}, \ i = 1, 2, ..., N. \tag{4}$$

Substituting the expression for F from (1) into (4), the governing equations can be written as

$$\frac{\partial \eta_i}{\partial t} = L\left(\kappa \nabla^2 \eta_i - \mu \eta_i (1 - \eta_i)(\alpha - \eta_i) - \lambda \eta_i \sum_{j>i} \eta_j^2\right),$$
$$i = 1, 2, ..., N. \tag{5}$$

The governing equation (5) is solved using a finite difference method and the active parameter tracking (APT) algorithm [17].

For a single circular nucleus in a deformed matrix, the equation (5) reduces to

$$\frac{\partial \eta_i}{\partial t} = L\left(\kappa \frac{\partial^2 \eta_i}{\partial r^2} + \frac{\kappa}{r}\frac{\partial \eta_i}{\partial r} - \mu \eta_i (1 - \eta_i)(\alpha - \eta_i)\right). \tag{6}$$

Following the work of Fan and Chen [21], we write $\partial \eta_i / \partial t = -v \partial \eta_i / \partial r$ in equation (6). Multiplying the resulting equation by $\partial \eta_i / \partial r$ and integrating with respect to r we obtain

$$v = L\left(-\frac{\kappa}{R} + \frac{\Delta f}{\beta}\right), \tag{7}$$

where $\beta = \int_0^\infty \left(\frac{\partial \eta_i}{\partial r}\right)^2 \mathrm{d}r$ and R is the position of the interface. In deriving the above equation, we have used the boundary conditions $\eta_i = 0$ and $\partial \eta_i / \partial r = 0$ for $r = 0$ and $r = \infty$.

The grain boundary mobility is a constitutive input into the phase field model. The boundary mobility depends on misorientation [25, 38, 39] and solute concentration [30]. In the present study, we take an alternative approach and use a mean-field mobility obtained from the experiments. In the following section, we discuss the mean field model used to obtain the experimental mobility parameter described.

4. Mean field model

In this section, we briefly summarise the mean field model proposed in [8]. The assumptions made in the development of mean field model are, (a) the deformed matrix is characterised by spatially uniform time dependent stored energy $E_{\mathrm{st}}(t)$, (b) uniform distribution of strain free nuclei of same size in the deformed matrix and (c) all nuclei grow at the same rate. The growth of the nuclei is modelled up to impingement which occurs at $\approx$70% area fraction. The initial critical radius of the nuclei is estimated from classical nucleation theory to be

$$R_C = \frac{2\gamma}{E_{\mathrm{st}}(0)}, \tag{8}$$

where γ is the grain boundary(GB) energy in $\mathrm{J\,m}^{-2}$ (For Ti, γ is taken as $0.7\,\mathrm{J\,m}^{-2}$ [22]).

Considering both the GB energy (γ) and time dependent deformation stored energy $E_{\mathrm{st}}(t)$, the net driving force (P) for the grain growth can be written as

$$P = \frac{-2\gamma}{R(t)} + E_{\mathrm{st}}(t), \tag{9}$$

where the first term is due to the curvature of the GB and $R(t)$ is grain radius as a function of time t. The velocity of the GB of a nucleus can be written in the classical form

$$v = MP = M\left(\frac{-2\gamma}{R(t)} + E_{\text{st}}(t)\right), \tag{10}$$

where M is the mobility and other terms are described above. During recovery, the stored energy of deformed matrix decreases due to thermal annihilation of dislocations. It is reasonable to expect that the stored energy decays exponentially and we write

$$E_{\text{st}}(t) = E_0 + E_1 \exp(-\vartheta t), \tag{11}$$

where E_0, E_1 and ϑ are the fitting parameters. Noting that the boundary velocity $v = \mathrm{d}R/\mathrm{d}t$, the governing equation for the growth of the nucleus can be written as

$$\frac{\mathrm{d}R}{\mathrm{d}t} = M\left(\frac{-2\gamma}{R(t)} + E_0 + E_1 \exp(-\vartheta t)\right). \tag{12}$$

Solving the above equation numerically using finite difference method for different M values and $R(t)$ (values greater than critical R_{C}), the variation of R with time can be obtained. The grain boundary mobility M was taken to be the value that best fits the experimental data of $R(t)$.

To estimate the recrystallised area fraction (area fraction is considered to be equal to volume fraction) from the grain radius R obtained from model, the following procedure is followed. For each deformation mode, for a given temperature and time, the area fraction recrystallised (A_{R}) is given by $A_{\text{R}(t)} = N_{\text{R}} \pi [R(t)]^2 / A_{\text{T}}$, where N_{R} is the number of recrystallised grains and A_{T} is the total area of microstructure considered for analysis. From the experimental data corresponding to approximately 70% recrystallisation (i.e. $A_{\text{R}} \approx 0.7$), the ratio of $N_{\text{R}}/A_{\text{T}}$ is obtained. The ratio obtained for a given deformation mode, strain and temperature was used to estimate the area fraction recrystallised from the grain radius obtained from mean field model.

In the following section we make use of the above developed mean field theory model to extract grain boundary mobilities during recrystallisation.

Note that comparing equation (7) with equation (10), the phase field parameters corresponding to the mean field model can be identified. Thus $L = M$, $\kappa = 2\gamma$ and $\Delta f = \beta E_{\text{st}}$ (t). The size of the growing nuclei with time is determined experimentally and used with the mean field model to obtain the mobility.

5. Results and discussion

Figures 1(a) and (b) show the inverse pole figures (IPF) of Ti samples deformed to equivalent strain of 0.5 through rolling and torsion respectively. The high angle grain boundary maps (marked in blue) superimposed with GOS $< 2°$ regions (marked in red) for these samples are shown in figures 1(c) and (d), respectively. Regions with GOS $< 2°$ represent strain free regions present in the deformed matrix and can be considered as potential nuclei. By analysing an area of $\sim 5000 \ \mu\text{m}^2$, the number of potential nuclei per unit area present in rolled and torsion deformed samples to equivalent strain of 0.5 are evaluated and presented in table 1. For the same strain, rolled samples have a higher number of potential nuclei per unit area than torsion deformed Ti samples. It may be noted that in our recent study on Ni [9], the growth of potential nuclei identified in the deformed matrix based on GOS $< 2°$ criterion was established by performing same area EBSD scans of deformed region and after short duration annealing treatment. In a study on Ti sample deformed through rolling and torsion to equivalent strain of 0.5, we found that the high angle grain boundary density and stored energy of plastic deformation in the rolled sample is higher than that of the torsion deformed
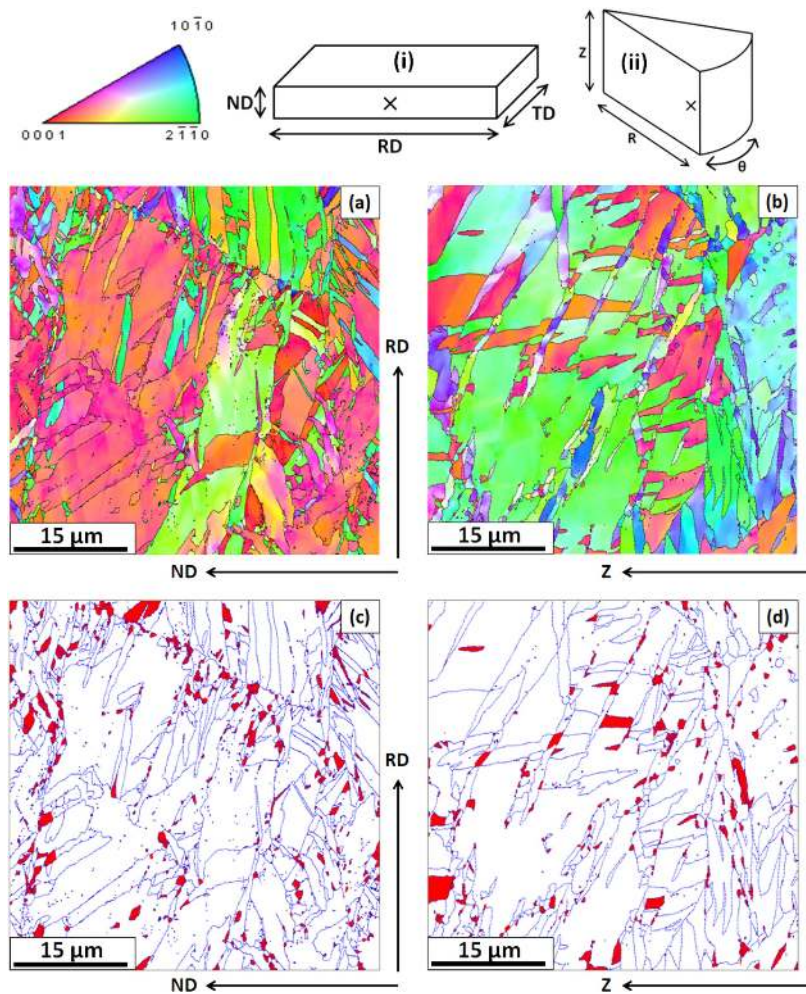
Figure 1. Schematic of cross sections of samples subjected to (i) rolling and (ii) torsion, region where EBSD analysis was performed is marked with X. Inverse pole figure (IPF) map of Ti sample deformed to equivalent strain of 0.5 through (a) rolling and (b) torsion, high angle grain boundary (in blue) map superimposed with GOS < 2° (in red) regions for Ti sample deformed to equivalent strain of 0.5 through (c) rolling and (d) torsion (RD: rolling direction, ND: normal direction, Z: axial direction, R: radial direction). The colour code in rolling and torsion correspond to RD-TD section and Z–θ section, respectively.

Table 1. Number of potential nuclei per unit area and stored energy of deformed Ti.

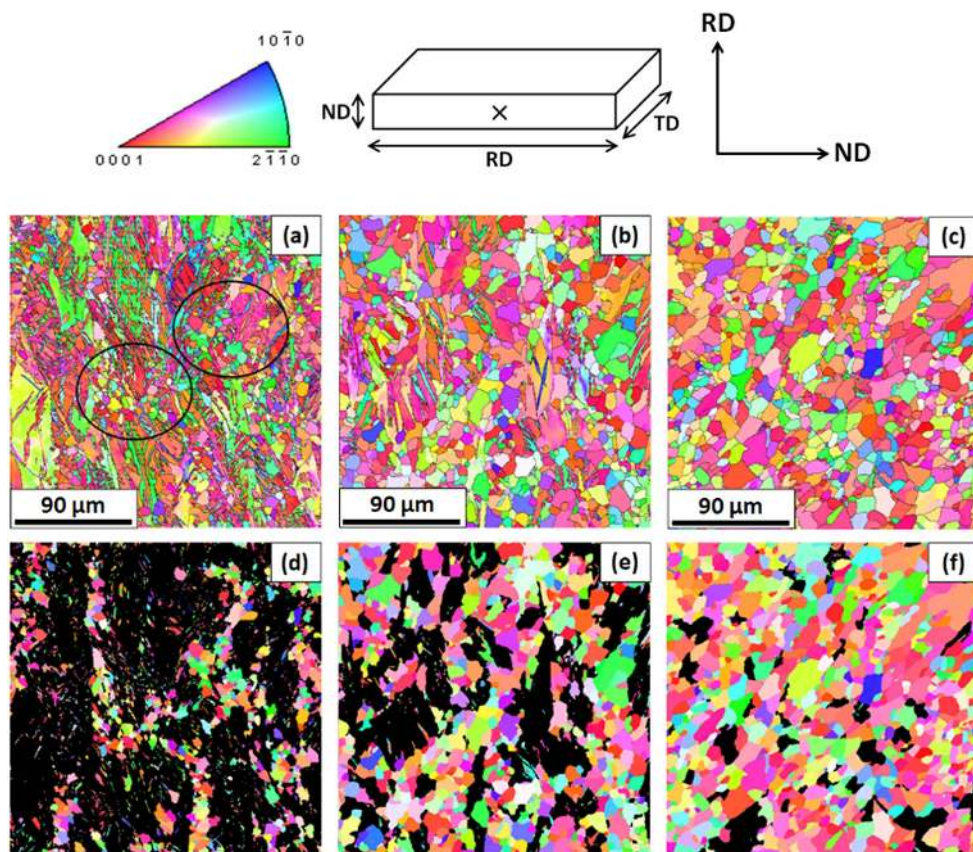| Deformation mode (equivalent strain)	Potential nuclei ($\times 10^5$ mm^{-2})	Stored energy (MJ m^{-3}) [17]
Rolling ($\varepsilon = 0.5$)	3.83 ± 0.75	2.4 ± 0.3
Torsion ($\varepsilon = 0.5$)	2.39 ± 1	2 ± 0.2

Figure 2. Inverse pole figure (IPF) maps of rolled samples deformed to an equivalent strain of $\varepsilon = 0.5$ and subjected to annealed at 848 K for (a) 600 s (b) 1800 s and (c) 3600 s. (d)–(f) show partitions of the recrystallised grains based on GOS $< 2°$ criterion from (a) to (c), respectively. The colour code corresponds to the RD-TD section.

sample [17]. The stored energies for rolled and torsion tested samples have been estimated from kernel average misorientations (KAM) (obtained from EBSD scans with step size of 300 nm) following the procedure outlined in [9, 40] and presented in table 1. From the above results it is reasonable to expect the recrystallisation kinetics to be faster in the rolled samples when compared to torsion deformed samples.

The evolution of microstructure during recrystallisation of rolled Ti sample at 848 K for different time durations is shown in figure 2. During the initial phase of recrystallisation (figure 2(a)), formation of nuclei in the form of clusters can be observed. With time, these nuclei grow and consume the deformed matrix (figures 2(b) and (c)). As the nucleation occurs in clusters, early grain impingement occurs within each cluster and results in concurrent grain growth within the clusters along with the recrystallisation in the deformed matrix. As a result, in the recrystallised microstructure, the distribution of both fine and coarse grains can be observed (figure 2(c)). In addition, small islands of deformed regions can also be observed in the recrystallised microstructure (in figure 2(c)). This is possibly due to concurrent occurrence of recovery in the deformed regions which leads to a decrease in the driving force needed for recrystallisation.
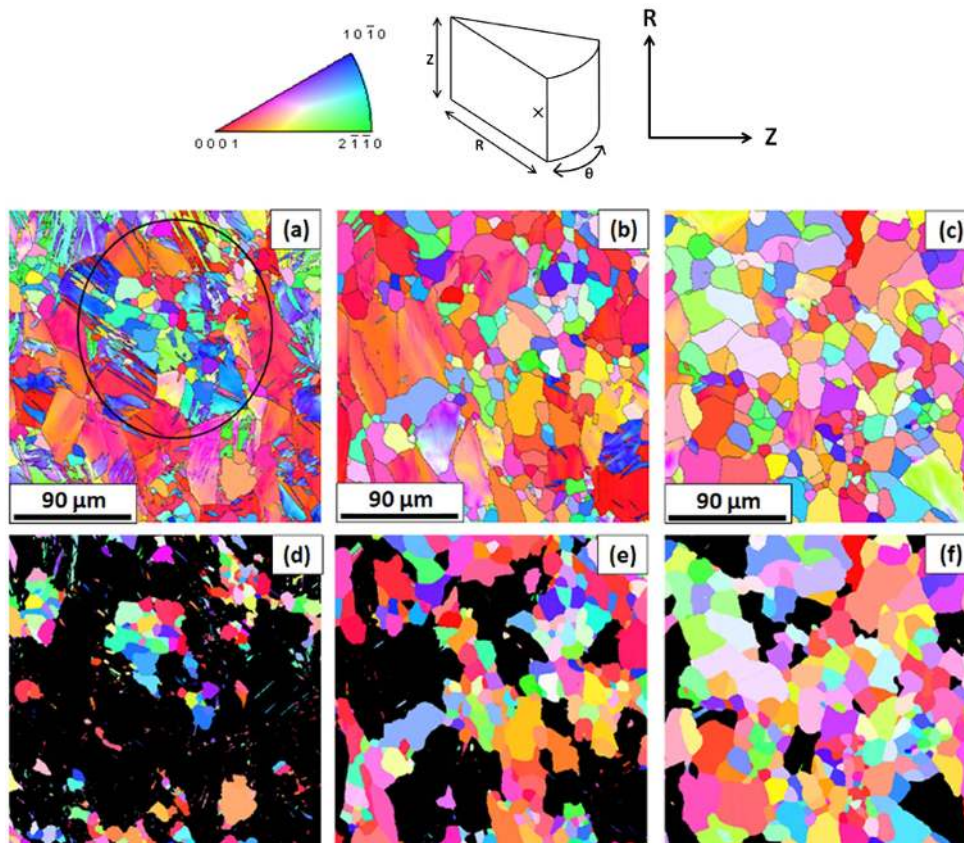
Figure 3. Inverse pole figure (IPF) maps of samples deformed through torsion to an equivalent strain of $\varepsilon = 0.5$ and subjected to annealed at 848 K for (a) 2700 s (b) 12 000 s and (c) 24 000 s. (d)–(f) show partitions of the recrystallised grains based on GOS $< 2°$ criterion from (a) to (c), respectively. The colour code corresponds to the Z–θ section.

The evolution of microstructure during annealing of torsion deformed Ti at 848 K is shown in figure 3. In the case of torsion deformed microstructure, there are two distinct regions viz., regions containing twins and regions deformed through slip [17]. During the initial stage of recrystallisation, recrystallisation nuclei have formed in the regions consisting of twins (encircled in figure 3(a)). Nucleation in the form of clusters, similar to those observed during recrystallisation of rolled samples, were also observed in torsion deformed samples. Regions with deformation twins are consumed first and regions without twins are consumed in the later stages of recrystallisation (figure 3(b)). The grains nucleated first continue to grow with time and hence both coarse and fine grains can be observed in the recrystallised microstructure (figure 3(c)).

Figure 4 shows the variation of recrystallisation fraction with time for rolled and torsion deformed samples (to equivalent strain of 0.5) annealed at 848, 873 and 898 K. For the given temperature, recrystallisation has occurred at much faster rate in rolled Ti samples compared to that of torsion deformed Ti samples. Faster recrystallisation kinetics in the case of rolled sample can be attributed to higher stored energy, higher number of potential nuclei per unit
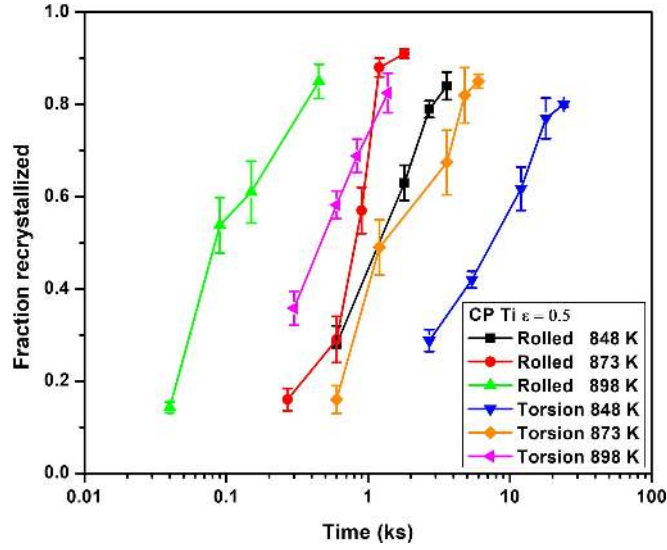
Figure 4. Recrystallisation kinetics of Ti samples deformed to equivalent strain of $\varepsilon = 0.5$ through rolling and torsion and subjected to annealing treatment at 848, 873 and 898 K.

area and higher fraction of high angle grain boundary density than torsion deformed sample [17].

The stored energies (E_{st}) were evaluated from the KAM obtained from EBSD through the expression [40]

$$E_{st} = \frac{\lambda \theta G b}{d}, \tag{13}$$

where λ is a constant which depends on the geometry of dislocation arrangements and is taken to be 3, θ is the average KAM in radians, the shear modulus $G = 44$ GPa and the Burger's vector $b = 0.412$ and 0.472 nm for rolled and torsion deformed sample respectively (average b from [17]), step size d is 300 nm. KAM value is step size dependent and hence a constant step size of 300 nm is used for all the measurements. The deformed microstructures consist of subgrains with their size typically less than a micrometre. In order to capture the contribution from misorientation due to subgrain boundary to stored energy, very fine step size scans of the order 50 nm or less is required. When the scans are run with coarser step size, contributions from the subgrain boundaries are excluded. The KAM of deformed sample decreases with increase in step size and hence it underestimates the stored energy. To capture statistically significant area with fine step sizes (50 nm or lower) requires very large time duration, hence a compromised step size of 300 nm was employed in the present study. For detailed analysis of different methods for estimation of stored energy of deformation from EBSD data and issues related to stored energy measurement from EBSD data, and for the dependence of KAM and stored energy on step size, the reader can refer to [41]. In the deformed material, both geometrically necessary dislocation (GNDs) and statistically stored dislocations (SSDs) contribute to the overall stored energy. Due to limitations pertaining to the angular resolution of EBSD technique, KAM based stored energy estimation accounts for contribution from GNDs alone. Based on GOS $> 2°$ criterion, deformed regions in partially recrystallised microstructures were partitioned and the stored energy was estimated from
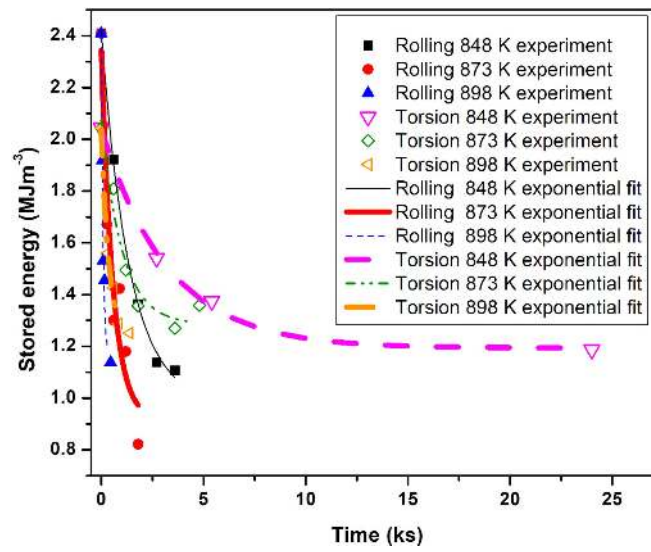
Figure 5. Decay of stored energy with time during annealing of rolled and torsion tested samples deformed to equivalent strains of 0.5 at 848, 873 and 898 K. The curves are fitted to exponential expression of the form $E_{st}(t) = E_0 + E_1 \exp(-\vartheta t)$.

Table 2. Fitting parameters for the evolution of stored energy for Ti samples annealed at 848, 873 and 898 K.

Deformation mode	Temperature (K)	E_0 (MJ m^{-3})	E_1 (MJ m^{-3})	ϑ (s^{-1})	Goodness of fit R^2
Rolling $\varepsilon = 0.5$	848	0.975	1.441	−0.000 73	0.99
	873	0.915	1.429	−0.001 79	0.87
	898	1.160	1.235	−0.0118	0.97
Torsion $\varepsilon = 0.5$	848	1.193	0.846	−0.000 31	0.99
	873	1.285	0.788	−0.001	0.93
	898	1.235	0.805	−0.002 82	0.98

KAM of the deformed regions during the progress of recrystallisation. From this data, it is possible to estimate decay in stored energy in the deformed regions with time. Figure 5 shows the variation of average stored energy with time in the deformed regions for the rolled and torsion deformed Ti samples subjected to annealing at 848, 873 and 898 K. The data were fit to the expression of the form $E_{st}(t) = E_0 + E_1 \exp(-\vartheta t)$ for each condition. The fitting parameters are presented in table 2.

The expression for the stored energy decay as a function of time are then substituted into equation (12) and solved numerically using finite difference method. The mobility coefficient is chosen such that the grain radius as a function of time matches the experimental data of average grain radius of recrystallised region corresponding to ∼70% recrystallisation fraction (figure 6(a)). The values of the mobility M from these calculations are presented in table 3. The match between the solution of the mean field equation and the experimental recrystallisation kinetics are shown in figure 6(b). Since the mean field model considers only the pre-impingement situation, the fits are shown up to ∼70% recrystallisation fraction. It can be
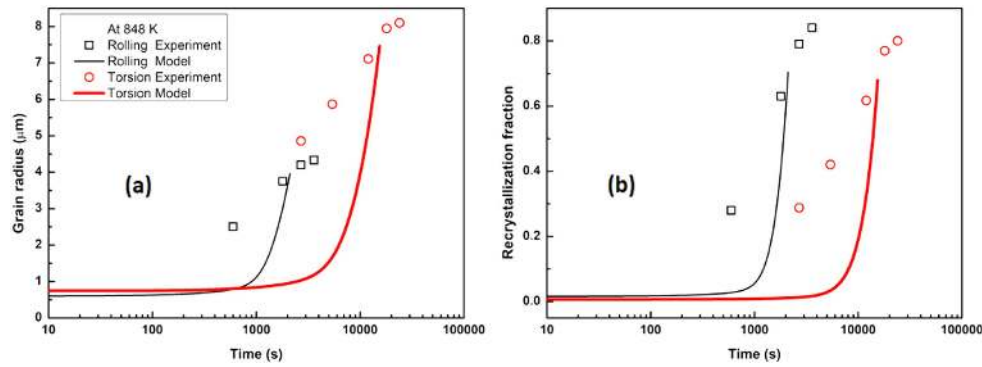
Figure 6. Mean field model fits of the grain growth based on (a) grain radius and (b) recrystallisation fraction for Ti samples annealed at 848 K.

Table 3. Mobility values calculated from the mean field model in rolled and torsion tested Ti samples subjected to an equivalent strain of 0.5.

| Temperature (K) | Mobility $M \times 10^{-15}$ (m^4 J^{-1} s^{-1}) | |
	Rolling $\varepsilon = 0.5$	Torsion $\varepsilon = 0.5$
848	3.29	0.68
873	5.4	2.23
898	25.5	9.15

seen that the match between the mean field model and the experiments is not particularly good and this could be attributed to several assumptions of idealised behaviour.

As mentioned above, the mean field model predicts growth behaviour only up to impingement. However, it is important to analyse and describe the entire recrystallisation process. In the present study, we use phase field simulations to describe entire recrystallisation process. To simulate microstructure evolution, nuclei identified based on GOS criterion from the experiments are used as input into the phase field model. To simulate microstructure and texture development during annealing, nuclei data from a relatively large area $500 \times 500 \, \mu m^2$ with fine step size ($\leqslant 50$ nm) is required and this is extremely time consuming. To get statistically significant data in reasonable time a larger step size is necessary. We have scanned large areas ($500 \times 500 \, \mu m^2$) using 300 nm step size. However, in scans of deformed samples run with 300 nm step size, it is not possible to identify and partition potential nuclei as majority of the nuclei are in the range of 100–200 nm in size. Deformed samples were therefore annealed for short duration. In case of rolling, sample annealed at 848 K for 600 s and in the case of torsion deformation, sample annealed at 848 K for 2700 s was used as input data for phase field simulation at other temperatures as well. Nuclei identified based on GOS < 2° were input to the phase field model to simulate microstructure and texture evolution during recrystallisation. The average orientation for each of the partitioned nuclei was determined and a single orientation was assigned for each nuclei. This was done for two reasons: (i) it is reasonable to assign average orientation to each nuclei since the orientation gradients are not significant, (ii) to update orientation during the growth of a nucleus in each time step of simulation, a single orientation value is needed. However, the

orientations of the deformed regions were not averaged. This was done in order to consider the heterogeneity in the stored energy.

Each identified nuclei was assigned a unique grain identification number and an order parameter η_i. The parameter α can be related to the stored energy by comparing equations (6) and (10)

$$\alpha = \frac{1}{2} - \frac{6E_{st}}{\mu}. \tag{14}$$

In the present work, the KAM distribution from experiment is taken as an input to the phase field model, therefore we use stored energy obtained from equation (13) and take $\alpha = 0.5 - \theta/12$ in the phase field simulations [8]. Typically, deformed regions in the microstructure are characterised by high KAM values, whereas KAM within strain free nucleus identified based on GOS criterion will have lower values and is taken as zero in the present study. During the simulation, KAM is updated at every time step by assigning value of zero to the newly grown regions in the microstructure.

In addition to the KAM data, the grain identification data from the EBSD scans are used as inputs to the phase field model. The mobilities calculated from the mean field model is another constitutive input to the model. 2D simulations were performed for both rolled and torsion deformed samples annealed at 848, 873 and 898 K. For each case, two sets simulations with domain size of 800×800 grid points and with a grid spacing of $\Delta x = \Delta y = 1$, assuming derivative boundary conditions. The simulation parameter used in the model are $\kappa = 2$, $\mu = 1$, $L = 2$, $\lambda = 1$. The time step of the phase field model is scaled using the experimental recrystallised data from the case of rolled $\varepsilon = 0.5$ sample annealed at 898 K. The scaled time step value $\Delta t = 0.125$ is used for the simulations of all the other conditions. Finally, the factor β defined by equation (7) depends on the thickness of the diffuse interface through κ, which is maintained constant throughout the domain by considering $\kappa/\Delta f$ to be constant [22]. Under these conditions, the width of each grain boundary is approximately 8 grid points.

The governing equation (5) with these simulation parameters is solved using a finite difference method. Further, we employed the APT algorithm [24] to enable the model to include large number of order parameters without increasing the computational cost. The APT algorithm is based on the idea that only the non-zero order parameters contribute to the evolution of the microstructure through the migration of interfaces. At each grid point, a set of ordered pairs contains the list of active order parameters whose magnitude is more than a small threshold value. In order to account for the possibility of a grain entering or leaving a computational point from neighbouring points active order parameters considering two levels of nearest neighbours are also added to the list. The order parameters from this list and their values are alone stored in the memory instead of storing all the order parameters. This significantly reduces the computational cost and time.

The microstructure obtained from the phase field simulations during annealing at 848 K of the rolled and torsion tested Ti samples are shown in figure 7. It can be seen that the phase field simulations captured the evolution of microstructure well (figures 2 and 3). The recrystallisation kinetics obtained from experiments and phase field simulations match to good accord (figure 8). The grain size distributions of the recrystallised grains (experimental and simulations) obtained from the partitioned microstructures (based on GOS $< 2°$ criterion) are shown in figure 9. Figures 9(a) and (b) show the experimental grain size distributions for the rolled and torsion tested samples. Figures 9(c) and (d) show the corresponding phase field simulation results. The results from phase field simulations peak agree reasonably well with the experimental results. The serrated shape observed in the grain size distribution obtained
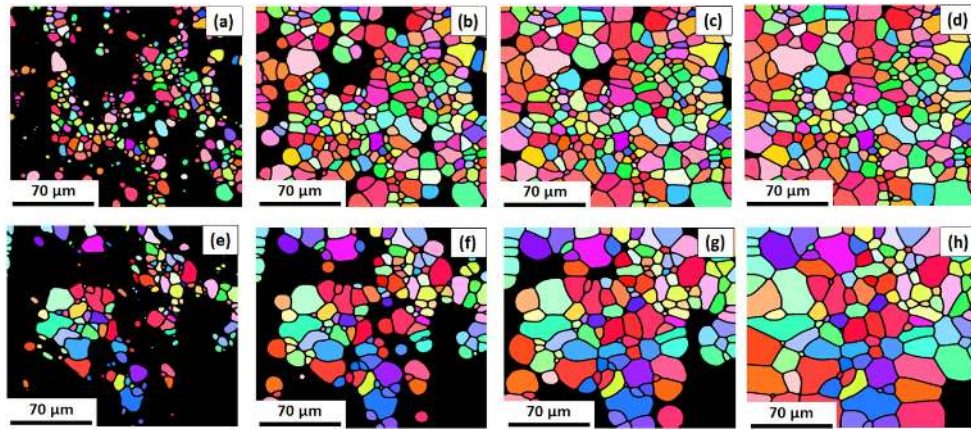
Figure 7. Phase field simulations of recrystallisation of rolled samples subjected to equivalent strain of $\varepsilon = 0.5$ during annealing at 848 K for (a) 600 s (input from experiment), (b) 1800 s, (c) 2700 s, and (d) 3600 s. Simulations of recrystallisation of torsion samples subjected to equivalent strain of $\varepsilon = 0.5$ during annealing at 848 K for (e) 2700 s (input from experiment), (f) 5400 s (g) 12 000 s and (h) 24 000 s. For rolling and torsion sample reference frame and colour code refer to figures 2 and 3, respectively.

from simulation is due to limited statistics as compared to experimental data. The average grain diameters after completion of recrystallisation of rolled and torsion deformed sample obtained from experiment and simulation are given in table 4. For a given equivalent strain of 0.5, recrystallisation of samples deformed through rolling has resulted in finer grain size as compared to torsion deformed sample. The finer grain size in the case of recrystallisation of rolled sample can be attributed to higher nuclei density, twin density and high angle grain boundary density than torsion deformed sample. Twin and high angle grain boundaries act as sites for recrystallisation nucleation. Twinning leads to grain subdivision and change in crystallographic orientation. The twin boundaries act as obstacles to deformation by slip and this results in accumulation of strain within twinned regions leading to increase in deformation heterogeneity [16]. As compared to the experimental results, the phase field simulations results overestimate the average grain size by a factor of $\sim$2. This is possibly due to the fact that mean field grain boundary mobility is used as constitutive input to the phase field model and the anisotropy in grain boundary mobility is not considered.

The activation energy Q of recrystallisation from experimental data is estimated from the expression

$$Q = RT\ln(Ct_{0.5}), \tag{15}$$

where R is the universal gas constant taken as 8.314 J mol^{-1} K^{-1}, T is the absolute temperature, C is a constant and $t_{0.5}$ is the time taken for 50% recrystallisation. Plot of ln $(t_{0.5})$ with $1000/T$ is shown in figure 10(a). The slope of the best fit lines give the activation energies for the rolled and torsion tested samples. The activation energies obtained from these plots are given in table 4. The activation energy of GB migration is calculated from Arrhenius type relation for the variation of the mobility M with $1/T$ by the relation
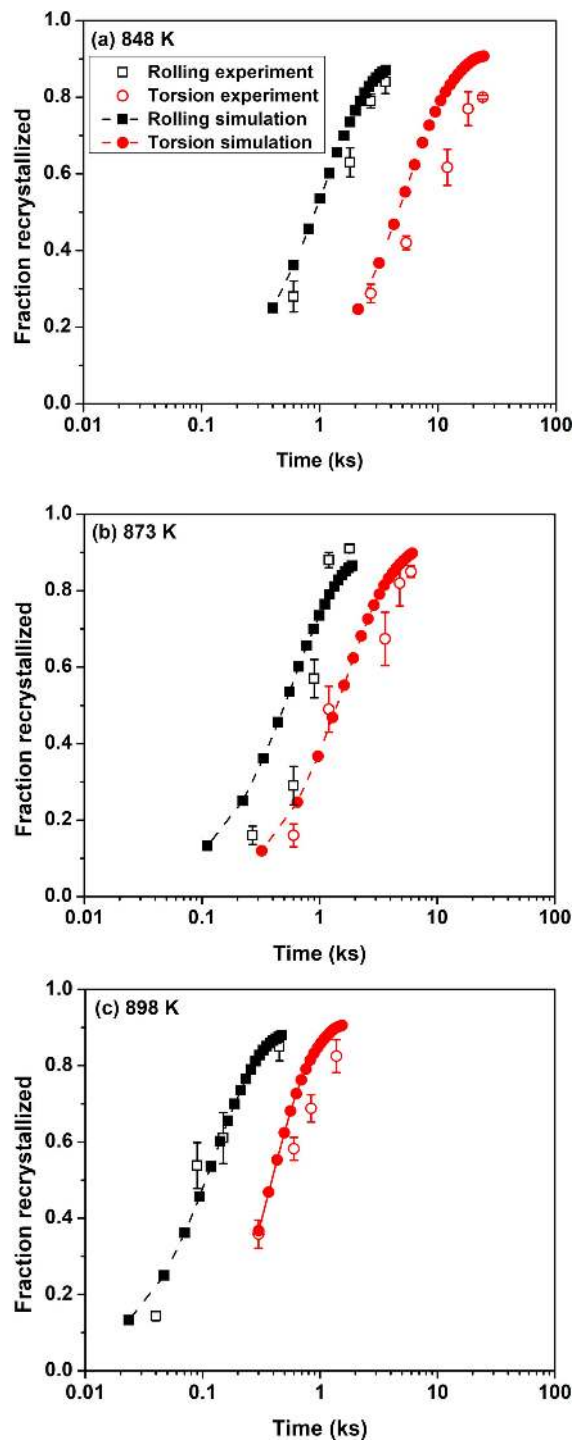
Figure 8. Comparison of experimental and phase field simulation results of recrystallisation fraction versus time during annealing at (a) 848 K (b) 873 K and (c) 898 K of rolled and torsion samples deformed to equivalent strain of $\varepsilon = 0.5$.
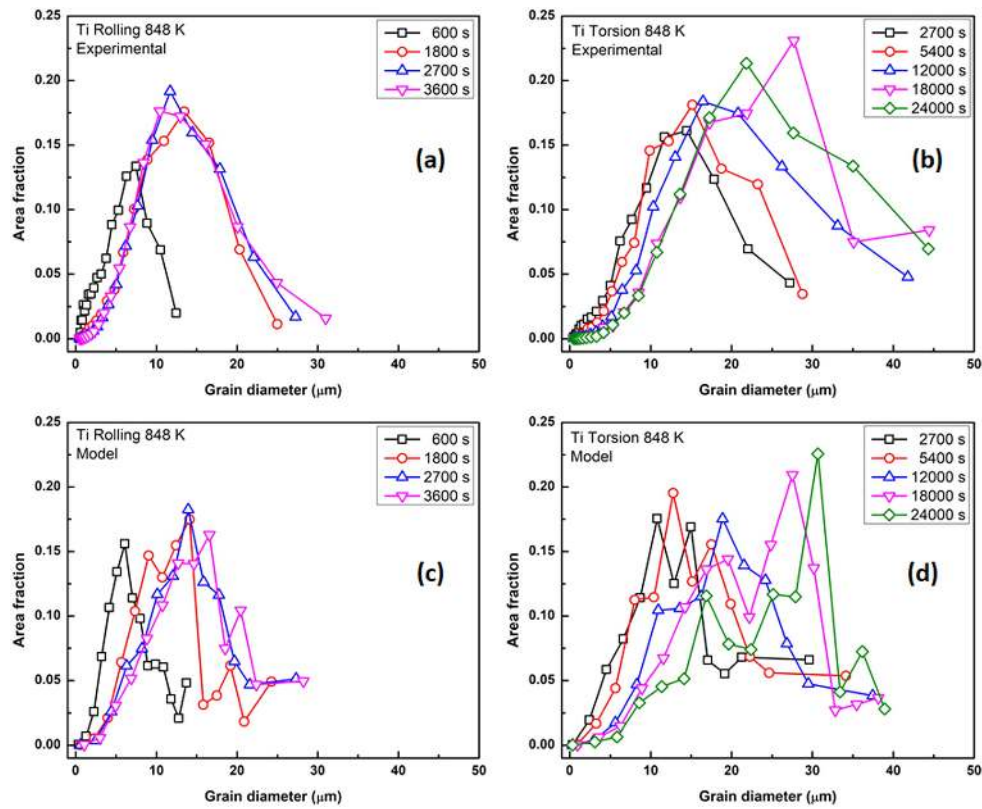
Figure 9. Experimental grain size distribution for Ti samples deformed to equivalent strain of 0.5 following annealed at 848 K for (a) rolling and (b) torsion. Grain size distribution from phase field simulations for (c) condition corresponding to (a) and (d) condition corresponding to (b), respectively.

Table 4. Recrystallisation time and average grain diameter of rolled and torsion tested samples following annealing at 848 K obtained from experiments and phase field simulations.

Deformation mode (equivalent strain)	Time (s)	Grain diameter (μm) (experiment)	Grain diameter (μm) (simulation)
Rolling ($\varepsilon = 0.5$)	3600	5.7	9.2
Torsion ($\varepsilon = 0.5$)	24 000	11.2	15.1

$$M = M_o \exp\left(\frac{-Q}{RT}\right). \qquad (16)$$

The activation energies of grain boundary migration obtained from the slope of the plot of M with $1/T$ (shown in figure 10(b)). The activation energies obtained from experimental recrystallisation kinetics and mobility calculation are in good agreement (table 5). This indicates that the mean field model captured the kinetics of recrystallisation to good accord.

Figures 11(a)–(c) show the (0002) pole figures of samples rolled to strain of 0.5, partitioned potential nuclei present in the as rolled microstructure and following annealing at
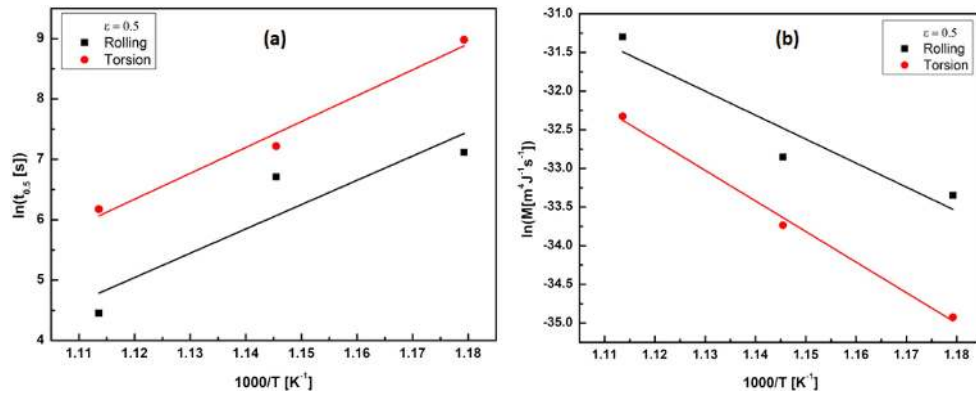
Figure 10. Plots of (a) time for 50% recrystallisation and (b) dependence of mobility with $1000/T$. The slopes of best fit lines give the activation energy.
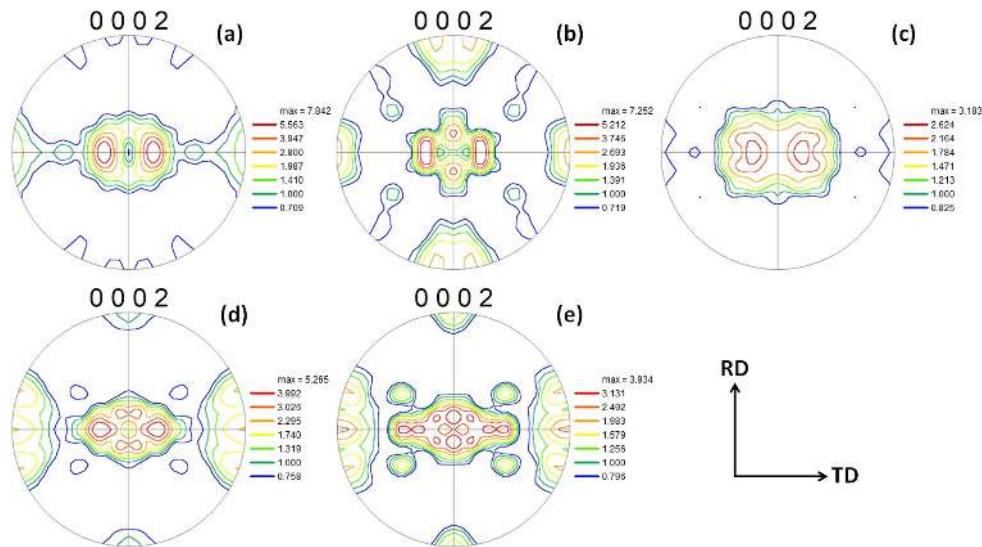

Figure 11. (0002) pole figure of (a) Ti sample deformed to equivalent strain of 0.5 through rolling, (b) orientation of potential nuclei identified based on GOS $< 2°$ in rolled sample deformed to equivalent strain of 0.5 and (c) after annealing at 848 K for 3600 s. (d) Sample annealed at 848 K for 600 s which is used as input data for phase field simulation and (e) texture obtained from phase field simulation at 848 K corresponding to 3600 s.

Table 5. Activation energies Q for two deformation modes obtained from experiments and mean field model.

	Rolling $\varepsilon = 0.5$	Torsion $\varepsilon = 0.5$
Experiment Q (kJ mol^{-1})	335	356
Model Q (kJ mol^{-1})	258	329

Table 6. Ideal deformation texture components for torsion in HCP materials.

Component	$(\phi_1, \varphi, \phi_2)°$	Description
B fibre	(0, 90, 0–60)	Basal plane || shear plane
P fibre	(0, 0–90, 30)	$\langle a \rangle$ || shear direction
Y fibre	(0, 30, 0–60)	c-axis rotated towards shear plane by 30°
C_1 and C_1 fibre	(60, 90, 0–60) and (120, 90, 0–60)	c-axis is first rotated 90° in shear direction and then ±30° in shear plane direction

848 K for 3600 s, respectively. In the rolled sample, split basal texture with basal plane rotated towards TD is observed. Split basal texture with 0002 pole making ±30° from ND towards TD is formed in HCP metals with $c/a < 1.633$ subjected to rolling [42–45]. During rolling of Ti, deformation occurs through slip up to around 10% reduction, followed by twinning up to 35%–40% reduction and finally by slip on further reduction. The formation of split basal texture is attributed to the formation of primary compressive twins followed by secondary tensile twins during the process of rolling. Strong split basal texture with other texture components are present in the potential nuclei obtained by partitioning using GOS < 2° criterion (figure 1(c)). It may be noted that this data is from small area scan of 5000 μm^2 run with step size 50 nm. Very limited changes have occurred in texture following recrystallisation and the rolling (split basal) texture is retained though texture strength has slightly weakened (figure 11(c)). The presence of split basal texture after recrystallisation of rolled sample indicates the preferred growth of the nuclei present in the deformed state during the recrystallisation. Occurrence of subgrain coalescence mechanism and its growth was shown to result in the retention of deformation texture component at the end of recrystallisation [46]. No significant change in texture is observed after recrystallisation and this could be due to the growth of identified potential nuclei having similar orientation as that of deformed grains. Wagner *et al* [42] have reported similar observations i.e., presence of split basal texture after recrystallisation of low alloyed Ti sheets rolled to 80% reduction. For the position of ideal shear texture component in HCP metals in a 0002 pole figure reader can refer to the work of Beausir *et al* [47]. The ideal components are listed in table 6. In all pole figures, the projection plane is the plane with normal R (the radial axis), the shear direction is horizontal (θ axis) towards the right and the axial direction (Z) is vertical. The pole figure of Ti sample through torsion to an equivalent strain of 0.5, partitioned potential nuclei present in the torsion deformed microstructure and for sample annealed at 848 K for 24 000 s is shown in figures 12(a)–(c), respectively. In sample deformed to equivalent strain of 0.5, strong B fibre is observed. The B fibre is 45° rotated about radial direction. B fibre is the stable end orientation in torsion deformed HCP metals [48]. Along with this, the deformed samples also consists of P, Y, C_1 and C_2 fibre components. The presence of C_1 fibre indicates the deformation activity by pyramidal $\langle c + a \rangle$ slip [47]. The texture of recrystallised sample is the similar to that of deformed sample. This is due to the growth of existing identified potential nuclei (figure 12(b)).

Texture evolution during recrystallisation for both rolled and torsion deformed samples was simulated using the phase field model. To simulate recrystallisation texture evolution, orientation changes of the strain free grains were tracked during the recrystallisation process for the duration of 3600 s and 24 000 s for rolling and torsion, respectively. The orientation data obtained from the simulations is compared with that of the experimental texture data of recrystallised sample. Figures 11(d) and (e) shows the (0002) pole figure of rolled sample annealed at 848 K for 600 s and pole figure obtained through simulation corresponding to
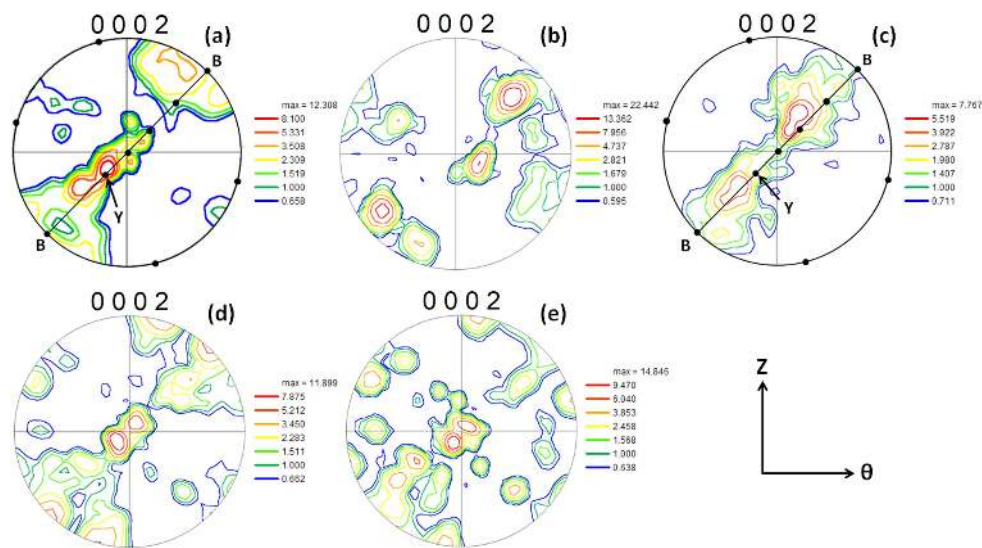
Figure 12. (0002) pole figure of (a) Ti sample deformed to equivalent strain of 0.5 through torsion, (b) orientation of potential nuclei identified based on GOS < 2° in torsion sample deformed to equivalent strain of 0.5, (c) after annealing at 848 K for 24 000 s. (d) Sample annealed at 848 K for 2700 s which is used as input data for phase field simulation and (e) texture obtained from phase field simulation at 848 K corresponding to 24 000 s.

3600 s, respectively. Even though the simulated recrystallisation texture consists of split basal texture component as observed in the experimental pole figure of recrystallised sample, it also contains other orientations as well.

Figures 12(c) and (d) shows the 0002 pole figure of torsion deformed sample annealed at 848 K for 2700 s and pole figure obtained through simulation corresponding to 24 000 s, respectively. As in the case of rolling, in case of torsion also, the recrystallisation texture predicted through phase field simulations compares well with experiments though few additional texture components are present in simulations. This is attributed to the anisotropy in grain boundary mobility which is not accounted for in the present study. In our simulation, we have used the same mean field grain boundary mobility for every boundary, whereas the grain boundary mobility is anisotropic and misorientation dependent. The stored energy distribution and recovery rate in the deformed microstructure is orientation dependent. The spatial spread of these orientations is non-uniform. The mean field model considers average stored energy and assumes uniform spatial distribution of stored energy. This limits the model's ability to capture anisotropy in boundary mobility. The additional texture components present in the simulations is attributed to the anisotropy in grain boundary mobility, which is not accounted for in the present simulation. The recrystallisation texture mainly depends on the orientation of nuclei and its ability to grow in the deformed matrix. Nucleation process is a localised event and in the present work, the assumption of site saturated nucleation (i.e. all nuclei are present at the deformed matrix and no new nuclei are formed during recrystallisation) is made for simulating microstructure through phase field model. This will also limit the model's ability to capture texture evolution completely. Therefore, there is a need to develop a model that is capable of capturing both fine scale events such as

nucleation and also operates on a large scale to consider a sufficiently large area to capture microstructure and texture evolution.

6. Conclusions

From the study on the influence of the mode of deformation (torsion and rolling) on recrystallisation behaviour of Ti through experiments and modelling, the following conclusions are obtained:

(a) Ti samples deformed through rolling recrystallised much faster than torsion deformed samples subjected to equivalent strain of 0.5. This is due to the higher stored energy, nuclei density and high angle grain boundary fraction in the rolled samples
(b) A phase field model with mean field grain boundary mobility as constitutive input is able to account for the observed differences in recrystallisation kinetics and predict the grain size distribution to good accord.
(c) The activation energy for grain boundary migration during recrystallisation of rolled and torsion deformed sample in the range of 848–898 K is comparable with activation energy of overall recrystallisation estimated from recrystallisation kinetics. Even though recrystallisation is faster in rolled samples than torsion deformed samples, the activation energy of recrystallisation rolled and torsion deformed samples are comparable.
(d) No significant change in deformation texture is observed after annealing for both rolled and torsion deformed samples. This is attributed to the growth of pre-existing nuclei present in the deformed matrix.
(e) The texture components predicted by the simulations and experimental pole figures of recrystallised samples show some differences. This may be due to anisotropy in the grain boundary mobility which is not considered in the phase field simulations.

ORCID iDs

C N Athreya ⬤ https://orcid.org/0000-0002-1129-2622

References

[1] Humphreys F J and Hatherly M 2004 *Recrystallization and Related Annealing Phenomena* (Oxford: Elsevier)
[2] Doherty R D, Hughes D A, Humphreys F J, Jonas J J, Jensen D J, Kassner M E, King W E, McNelley T R, McQueen H J and Rollett A D 1997 Current issues in recrystallization: a review *Mater. Sci. Eng.* A **238** 219–74
[3] Barto R L and Ebert L J 1971 Deformation stress state effects on the recrystallization kinetics of molybdenum *Metall. Trans.* **6** 1643–9
[4] Cowan J R, Higginson R L, Hutchinson W B and Bate P S 1995 Recrystallisation following non-proportional straining in aluminium *Mater. Sci. Technol.* **11** 1104–9

[5] Mishra S K, Tatiparti S S V, Tiwari S M, Raghavan R S, Carsley J E and Li J 2013 Annealing response of AA5182 deformed in plane strain and equibiaxial strain paths *Phil. Mag.* **93** 2613–29

[6] McDonald D T, Bate P S and Hutchinson W B 2005 Effect of strain path change on recrystallisation in copper *Mater. Sci. Technol.* **21** 693–700

[7] Molodova X, Gottstein G, Winning M and Hellmig R J 2007 Thermal stability of ECAP processed pure copper *Mater. Sci. Eng.* A **460–461** 204–13

[8] Athreya C N, Mukilventhan A, Suwas S, Vedantam S and Subramanya Sarma V 2017 Influence of the mode of deformation on recrystallisation kinetics in nickel through experiments, theory and phase field model *Phil. Mag.* **97** 3211–28

[9] Athreya C N, Suwas S and Subramanya Sarma V 2015 Influence of mode of deformation on microstructural heterogeneities in Ni subjected to large strain deformation *Phil. Mag. Lett.* **95** 441–9

[10] Sahoo S K, Sabat R K, Sahni S and Suwas S 2016 Texture and microstructure evolution of commercially pure titanium during hot rolling: role of strain-paths *Mater. Des.* **91** 58–71

[11] Sinha S, Ghosh A and Gurao N P 2016 Effect of initial orientation on the tensile properties of commercially pure titanium *Phil. Mag.* **96** 1485–508

[12] Sahoo S K, Sabat R K, Bishoyi B D, Anjani A G S and Suwas S 2016 Effect of strain-paths on mechanical properties of hot rolled commercially pure titanium *Mater. Lett.* **180** 166–9

[13] Sinha S, Pukenas A, Ghosh A, Singh A, Skrotzki W and Gurao N P 2017 Effect of initial orientation on twinning in commercially pure titanium *Phil. Mag.* **97** 775–97

[14] Won J W, Park C H, Hong S-G and Lee C S 2015 Deformation anisotropy and associated mechanisms in rolling textured high purity titanium *J. Alloys Compd.* **651** 245–54

[15] Salem A A, Kalidindi S R and Doherty R D 2003 Strain hardening of titanium: role of deformation twinning *Acta Mater.* **51** 4225–37

[16] Won J W, Lee T, Hong S-G, Lee Y, Lee J H and Lee C S 2016 Role of deformation twins in static recrystallization kinetics of high-purity alpha titanium *Met. Mater. Int.* **22** 1041–8

[17] Athreya C N, Kapoor G, Gubicza J and Subramanya Sarma V 2017 Influence of mode of plastic straining on the microstructure of Ni and Ti deformed through rolling and torsion *Mater. Charact.* **132** 205–14

[18] Raabe D 2002 Cellular automata in materials science with particular reference to recrystallization simulation *Annu. Rev. Mater. Res.* **32** 53–76

[19] Rollett A D, Srolovitz D J, Doherty R D and Anderson M P 1989 Computer simulation of recrystallization in non-uniformly deformed metals *Acta Metall.* **37** 627–39

[20] Moelans N, Godfrey A, Zhang Y and Juul Jensen D 2013 Phase-field simulation study of the migration of recrystallization boundaries *Phys. Rev.* B **88** 1–10

[21] Moelans N, Zhang Y B, Godfrey A and Juul Jensen D 2015 A phase-field simulation study of irregular grain boundary migration during recrystallization *IOP Conf. Ser.: Mater. Sci. Eng.* **89** 12037

[22] Gentry S P and Thornton K 2015 Simulating recrystallization in titanium using the phase field method *IOP Conf. Ser.: Mater. Sci. Eng.* **89** 12024

[23] Fan D and Chen L-Q 1997 Computer simulation of grain growth using a continuum field model *Acta Mater.* **45** 611–22

[24] Vedantam S and Patnaik B S V 2006 Efficient numerical algorithm for multiphase field simulations *Phys. Rev.* E **73** 16703

[25] Upmanyu M, Srolovitz D J, Shvindlerman L S and Gottstein G 1999 Misorientation dependence of intrinsic grain boundary mobility: simulation and experiment *Acta Mater.* **47** 3901–14

[26] Tonks M R, Zhang Y, Biner S B, Millett P C and Bai X 2013 Guidance to design grain boundary mobility experiments with molecular dynamics and phase-field modeling *Acta Mater.* **61** 1373–82

[27] Zhou J and Mohles V 2011 Towards realistic molecular dynamics simulations of grain boundary mobility *Acta Mater.* **59** 5997–6006

[28] Molodov D A, Swiderski J, Gottstein G, Lojkowski W and Shvindlerman L S 1994 Effect of pressure on grain boundary migration in aluminium bicrystals *Acta Metall. Mater.* **42** 3397–407

[29] Vandermeer R A, Jensen D J and Woldt E 1997 Grain boundary mobility during recrystallization of copper *Metall. Mater. Trans.* A **28** 749–54

[30] Huang Y and Humphreys F J 2012 The effect of solutes on grain boundary mobility during recrystallization and grain growth in some single-phase aluminium alloys *Mater. Chem. Phys.* **132** 166–74

[31] Ateba Betanda Y, Helbert A-L, Brisset F, Waeckerlé T and Baudin T 2015 Effect of annealing atmosphere on the recrystallized texture and abnormal grain growth of Ni–5%W alloy sheets *Adv. Eng. Mater.* **17** 1568–72

[32] Bernard P, Bag S, Huang K and Logé R E 2011 A two-site mean field model of discontinuous dynamic recrystallization *Mater. Sci. Eng.* A **528** 7357–67

[33] Favre J, Fabrègue D, Piot D, Tang N, Koizumi Y, Maire E and Chiba A 2013 Modeling grain boundary motion and dynamic recrystallization in pure metals *Metall. Mater. Trans.* A **44** 5861–75

[34] Hillert M 1965 On the theory of normal and abnormal grain growth *Acta Metall.* **13** 227–38

[35] Hurley P J and Humphreys F J 2003 Modelling the recrystallization of single-phase aluminium *Acta Mater.* **51** 3779–93

[36] Zhu B and Militzer M 2012 3D phase field modelling of recrystallization in a low-carbon steel *Model. Simul. Mater. Sci. Eng.* **20** 85011

[37] Darvishi Kamachali R, Kim S-J and Steinbach I 2015 Texture evolution in deformed AZ31 magnesium sheets: experiments and phase-field study *Comput. Mater. Sci.* **104** 193–9

[38] Kazaryan A, Wang Y, Dregia S A and Patton B R 2002 Grain growth in anisotropic systems: comparison of effects of energy and mobility *Acta Mater.* **50** 2491–502

[39] Taheri M L, Molodov D, Gottstein G and Rollett A D 2005 Grain boundary mobility under a stored-energy driving force: a comparison to curvature-driven boundary migration *Z. Met.* **96** 1166–70

[40] Takayama Y and Szpunar J A 2004 Stored energy and Taylor factor relation in an Al–Mg–Mn alloy sheet worked by continuous cyclic bending *Mater. Trans.* **45** 2316–25

[41] Godfrey A, Mishin O V and Yu T 2015 Characterization and influence of deformation microstructure heterogeneity on recrystallization *IOP Conf. Ser.: Mater. Sci. Eng.* **89** 12003

[42] Wagner F, Bozzolo N, Van Landuyt O and Grosdidier T 2002 Evolution of recrystallisation texture and microstructure in low alloyed titanium sheets *Acta Mater.* **50** 1245–59

[43] Tenckhoff E 2005 Review of deformation mechanisms, texture, and mechanical anisotropy in zirconium and zirconium base alloys *J. ASTM Int.* **2** 25–50

[44] Zhong Y, Yin F and Nagai K 2008 Role of deformation twin on texture evolution in cold-rolled commercial-purity Ti *J. Mater. Res.* **23** 2954–66

[45] Ghosh A, Singh A and Gurao N P 2017 Effect of rolling mode and annealing temperature on microstructure and texture of commercially pure-titanium *Mater. Charact.* **125** 83–93

[46] Zhu K Y, Chaubet D, Bacroix B and Brisset F 2005 A study of recovery and primary recrystallization mechanisms in a Zr–2Hf alloy *Acta Mater.* **53** 5131–40

[47] Beausir B, Tóth L S and Neale K W 2007 Ideal orientations and persistence characteristics of hexagonal close packed crystals in simple shear *Acta Mater.* **55** 2695–705

[48] Biswas S, Beausir B, Toth L S and Suwas S 2013 Evolution of texture and microstructure during hot torsion of a magnesium alloy *Acta Mater.* **61** 5263–77